2024, 21(9): 2838-2852
https://doi.org/10.21123/bsj.2024.8591
P-ISSN: 2078-8665 - E-ISSN: 2411-7986
Baghdad Science Journal

Removal of Some Heavy Metals from Polluted Water Using New Schiff Base for Polyacrylamide with Zeolite Nanocomposites

***Zainab Sabeer Abdulsada* *[1], *Sahar S. Hassan* [2], *Sanaa Hitur Awad*[2]**

[1]Ministry of Environment, Baghdad, Iraq.
[2]Department of Chemistry, College of Science for Women, University of Baghdad, Baghdad, Iraq.
*Corresponding Author.

Received 14/02/2023, Revised 16/07/2023, Accepted 18/07/2023, Published Online First 20/02/2024, Published 01/09/2024

© 2022 The Author(s). Published by College of Science for Women, University of Baghdad.
This is an open-access article distributed under the terms of the Creative Commons Attribution 4.0 International License, which permits unrestricted use, distribution, and reproduction in any medium, provided the original work is properly cited.

Abstract

This work involved the preparation of a new Schiff base ligand derived from poly acrylamide and glutaraldehyde [(2S, 2'S) – N, N' - (pentane-1, 5-diylidene) bis (2- methylbutan amide)] (PAAG) with some heavy metals (Cr +3, Mn + 3, Fe + 3, Co + 2, Ni + 2, Cu + 2, Zn + 2, Cd + 2) to produce corresponding complexes. Schiff bases and their metal complexes are characterized using FTIR spectral, Uv-Vis spectroscopy, conductivity, magnetic moments, Thermal gravimetric analysis (TGA), x-ray diffraction, scanning electron microscope (SEM) and atomic force microscope (AFM). The prepared polymer was used with zeolite to form composite material to remove some of the elements from polluted water that were drawn from industrial water of the electric power plants in Dora and South Baghdad. Also, estimate the elements trace concentrations before and after using the prepared base by atomic absorption spectroscopy.

Keywords: Acrylamide, Composite materials, contaminated water, Schiff base, Zeolite.

Introduction

The health risks associated with contaminated water continue to be an international concern[1]. Due to their toxicity, non-biodegradability, and bioaccumulation in the food chain, metal poisoning poses a significant threat[2]. Heavy metal pollution in water supplies is mainly caused by industrial garbage. Negative and direct effects on flora and fauna make the successful removal of harmful ions from wastewater an urgent and essential issue[3]. The carcinogenic effects of heavy metals are exacerbated in animals and humans through the food chain, where they are ingested by those species[4]. Plants absorb these metals and pass them on to animals and humans. Many industries use acrylamide (AA), a highly reactive chemical molecule that may be polymerized to generate polyacrylamide. Research on AA has intensified over the past 20 years because of the toxicity it poses to people and animals. Food sources are significant in the production of AA; the International Agency for Research on Cancer (IARC) designated acrylamide as a possible human carcinogen in 1994[5]. At least four decades have passed since polymers were first used in water purification techniques. Utilizing them has several benefits, including less sludge production, a decrease in the ionic load of the treated water, less aluminum in the water, and lower costs. Polymers used for water purification are soluble and may be classified into three main ionic groups: cationic, anionic, and non-ionic[6]. Polyamides (PAs) are a widely used type of synthetic polymer with significant economic significance. In particular, the hydrogen bonding between the amide groups and the

other atoms in the chain gives them their usefulness. Higher glass transition temperatures and melting points can be attributed to these hydrogen-bonding interactions. The bulk of PAs is made by either a condensation polymerization method involving the reaction of diamines with dicarboxylic acid derivatives or a chain growth method involving the ring-opening polymerization of cyclic amides[7]. The carboxyl group on polyacrylamide is complexed with inorganic cross-linking systems, whereas the amide group is primarily reacted with by organic cross-linking systems, leading to a water-insoluble three-dimensional network structure[8]. Polyacrylamide is one of the most versatile polymers available, having uses varying from sub-dermal filler in cosmetic surgery, wastewater treatment of oil recovery[9], soil conditioning, agriculture, biochemistry, and medicinal applications[10]. Zeolite, an aluminosilicate mineral, is widely used in the chemical industry as a surfactant. Swedish mineralogist Axel Fredrik Cronstedt coined the term "zeolite" in 1756; the word "zeolite" comes from the Greek zéo, which means "boiling," and lithos, which means "stone."[11]. The widely known chemical formula for synthetic sodium cation zeolite A is:

$$Na_{12}\,[AlO_2.\ SiO_2]12.\ 27H_2O$$

Type A of zeolite is subdivided into three classes, 3A, 4A, and 5A, all share the same public formula but contain distinctive cation compositions. It is considered zeolite when 75% of sodium is replaced by potassium (3A). Instead, zeolite (5A) is formed when calcium is exchanged[12]. Zeolites' cationic exchange negative charge features and inexpensive production make them promising for eliminating many contaminants, including toxic metals, chemical compounds, dyes and pigments, reagents, and nitrogen compounds [13].

Materials and Methods

Acrylamide was provided by (Riedel-De Haen Ag Seelze- Hannover), Absolute Ethanol (B.D.H), glutaraldehyde was provided by (SIGMA), and ($CrCl_3.H_2O$, $MnCl_2.4H_2O$, $FeCl_3$, $CoCl_2.6H_2O$, $NiCl_2.6H_2O$, $CuCl_2.2H_2O$, $ZnCl_2$, and $CdCl_2.H_2O$) was provided by (B.D.H).

Instruments

GM Mallen Kampm was used to measure the melting points of the synthesized compounds. MF-370 devised electro-thermal at the University of Baghdad, College of Sciences for Women. Fourier Transform Infrared (FTIR) spectra were obtained using a SHIMADZUE FT-IR 8400S Fourier transform within the wavenumber region between 4000-400 cm^{-1} using a KBr disc and 4000-200 cm^{-1} using a CsI disc. Electronic spectra for compounds in the (UV-Visible) region (200-1100) nm were recorded using a SHIMADZUE 1800 Double Beam UV-Visible spectrophotometer; all were done at the University of Baghdad.^{1}H-NMR performed using a Bruker Ultra Sheild 300 MHz NMR in Taban Lab, Iran. Thermal analyses (TGA) of samples were performed under nitrogen atmospheres at a heating range of 25-900˚C and a heating rate of 20˚C/min. using SDT Q600 V20.9 Build 20 in Taban Lab, Iran. Molar conductivity measurements ($\mu s.cm^{-1}$) for metal complexes (10^{-3} M) in Ethanol at room temperature were carried out using LASSCO Digital Conductivity Meter. Magnetic moments (eff. B.M) for the prepared complexes in the solid state at room temperature were measured according to Faraday's method using Bruker Magnet B.M-6, Atomic Absorption measurements were performed using BUCK Scientific model 210 VGP USA Atomic Absorption Spectrophotometer.

Synthesis

Synthesis of [(2S, 2'S) – N, N' - (pentane-1, 5-diylidene) bis (2- methylbutan amide)] (PAAG) ligand

Around the bottom flask, 10gm of Acrylamide was mixed with (0.5gm di-benzoyl peroxide as an initiator at 70°C. The mixture was heated in a water bath and continuously stirred for 6 h to separate the homo polymer of PAAm[14, 15]. The reaction mixture was allowed to cool to ambient temperature; the product was washed with diethyl ether and dried in an oven at 50°C for 1 hr. The vicious white polymer was obtained with 55%. The steps of polymerization are shown in Scheme 1. In the second step, a Schiff base was prepared by dissolving polyacrylamide (1.0 g, 0.0142 mol) in absolute ethanol (99.95%) (5mL), then adding three drops of glacial acetic acid and stirring continuously at room temperature 25ºC. After diluting with absolute ethanol (5 mL), glutaraldehyde (2 mL, 0.0149 mol) was added, and the mixture was refluxed with constant stirring at 45°C for 12 hrs. in a water bath[16, 17]. The product was

2024, 21(9): 2838-2852
https://doi.org/10.21123/bsj.2024.8591
P-ISSN: 2078-8665 - E-ISSN: 2411-7986
Baghdad Science Journal

then dried at room temperature for a whole night before being washed with diethyl ether Scheme 1.

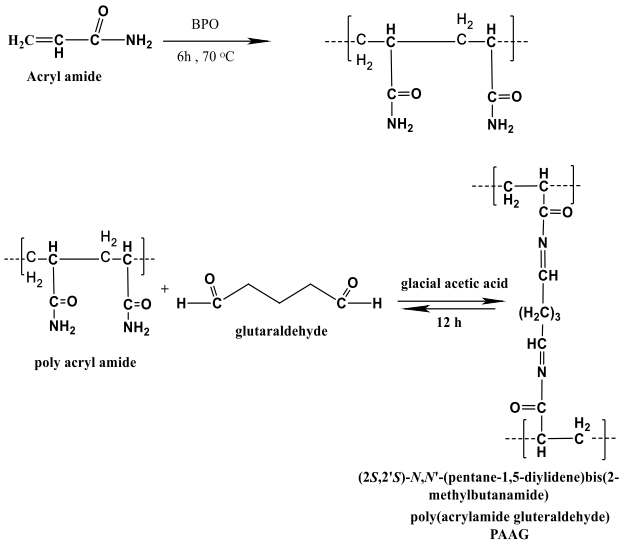

Scheme 1. Preparation of polyacrylamide-glutaraldehyde (PAAG) ligand

Synthesis of (2S, 2'S) – N, N' - (pentane-1, 5-diylidene) bis (2- methylbutanamide) (PAAG) ligand complexes

The ligand of polyacrylamide-glutaraldehyde (PAAG) complexes were prepared at a ratio of 2:1 from the ligand to the element; ligand (0.106 g, 0.002 mol) was dissolved in distilled water 5 mL and ethanol 20 mL with continuous stirring in a condensation flask until it dissolved, and then was added solution of metal chloride salt (0.001 mol, 1.0 eq) in ethanol 10 mL. The mixture was refluxed for 3 hrs. The product was placed in a watch glass and let dry at room temperature.

Results and Discussion

FTIR Spectra of ligand and its metal complexes

Specific vibrations of chemical bonds or functional groups within molecules were reflected as peaks in FTIR spectra [18]. It is shown in Fig. 1. that KBr FTIR spectroscopy in the range of 4000-400 cm^{-1} and CsI FTIR spectroscopy in the range of 4000-250 cm^{-1} were used to determine the experimental and theoretical structure of the (PAAG) polymer complexes.

In the prepared ligand, several peaks that belonged to the C=O and C=N groups at the wave numbers 1639 and 1558 cm^{-1}, respectively, appeared. When the complexes were formed, a change occurred in these wave numbers to lower frequencies with limits from 18-35 cm^{-1} for ν (C=O) and to higher frequencies with limits from 4-46 cm^{-1} for ν (C=N)[19, 20]. That was because the band mentioned previously was shifted to a lower wave number in all complexes indicating that the imine group was involved in complex coordination through the nitrogen atom (C=N→M) with the metal ion; new bands observed at 418-457 cm^{-1}were appointed to the υ (M–N), and bands that emerge at 501–574 cm^{-1} were attributed to ν (M-O) [21]. The υ(M-Cl) bands appeared at ~325 cm^{-1} [22], as seen in Table. 1 and Fig. 1. The coordination of the metal ion to the nitrogen of the Schiff base and the carbonyl oxygen of the carboxylate group could account for these frequency shifts relative to the bands of the polymeric Schiff bases. For polymeric Schiff bases, the bands at 1413 cm^{-1} can be attributed to (C-N) [23]; simultaneously, bands in the 3440–3442 cm^{-1} were assigned to ν (OH) modes. The PAAG-Schiff base behaved as a neutral bidentate ligand, with metal (II) and metal (III) ions bonding with once nitrogen and once carbonyl oxygen.

2024, 21(9): 2838-2852
https://doi.org/10.21123/bsj.2024.8591
P-ISSN: 2078-8665 - E-ISSN: 2411-7986
Baghdad Science Journal

Table 1. The FT-IR spectrum of the L synthesized ligand and its complexes.

Compound	υ(H_2O) Lattice	υ(C=O) amide	υ(C=N)	υ(C-N)	υ(M-N)	υ(M-O)	υ(M-Cl)
L	3429	1639	1558	1413	-	-	
CrL	3440	1622	1602	1442	418	509	325
MnL	3446	1623	1602	1456	418	574	329
FeL	3444	1612	1560	1458	420	516	327
CoL	3438	1622	1602	1452	410	501	325
NiL	3425	1623	1602	1456	420	511	329
CuL	3446	1629	1562	1413	437	552	327
ZnL	3448	1604	1604	1460	457	532	327
CdL	3560	1622	1585	1435	416	530	329

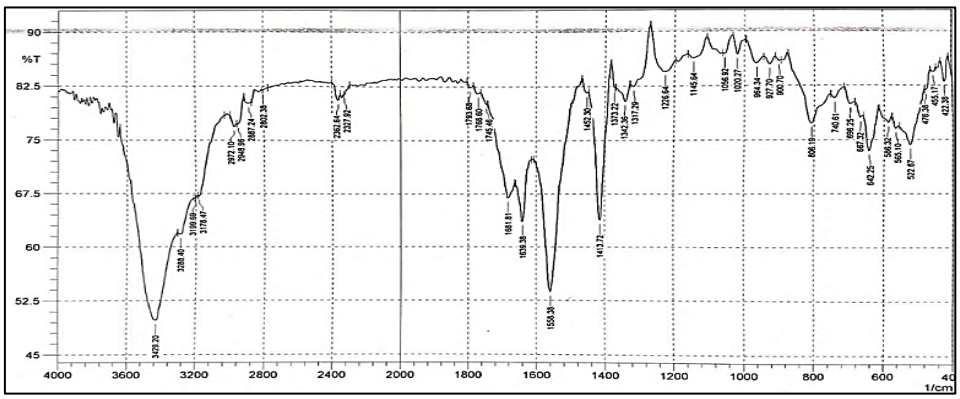

(a)

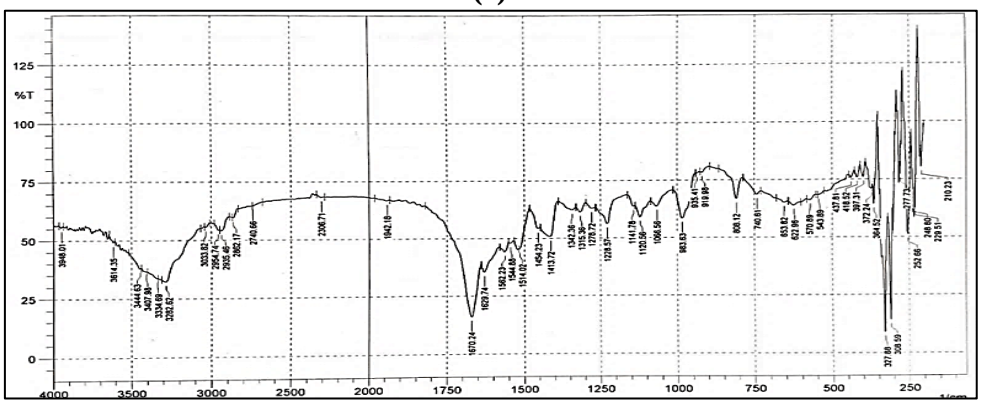

(b)

Figure 1. The FTIR Spectra for (a) PAAG-L (b) CuL

2024, 21(9): 2838-2852
https://doi.org/10.21123/bsj.2024.8591
P-ISSN: 2078-8665 - E-ISSN: 2411-7986
Baghdad Science Journal

The electronic spectra (UV-Vis) of ligands and their complexes:

Intense absorption at 273 nm (36630) cm^{-1} in the UV-Vis spectrum of Schiff base (PAAG) - ligand is ascribed to the (n→π*) transition, while intense absorption at 231,212 nm (43290, 47170) cm^{-1} was ascribed to the (π→ π*) transition Fig. 2. In Table 3 information on the spectra, molar conductivity of all metal complexes of the (PAAG) - ligand in ethanol, and the values of magnetic moments was described.

Cr (III): the first transition υ_1 taken from the IR spectrum and found to be 3438 cm^{-1} Scheme 3 (b) Spectrum of Cr (III) complex olive color (CrL) showed three absorption bands at 820, 670, and 460 nm (12195,14925 and 21739) cm^{-1} were assigned to $^4A_2g \rightarrow {}^4T_2g$, $^4A_2g_{(F)} \rightarrow {}^4T_1g$ and $^4A_2g_{(F)} \rightarrow {}^4A_2g$ transitions. The magnetic moment was 3.8 BM, suggesting an octahedral geometry [24].

For the Mn (II)-PAAG complex, three bands of complexes were uncultivated:

Three bands corresponding to $^6A_1g \rightarrow {}^4T_1g$ (G), $^6A_1g \rightarrow {}^4T_2g$ (G), and $^6A_1g \rightarrow {}^4A_2g + Eg$ (G) were seen at 11765, 19231, and 26316 cm^{-1} [25]; the magnetic moment was 5.1 BM.

The spectrum of Fe (III) complex brown color (FeL) showed three bands at 701, 590, and 339 nm (14265, 16949, and 29499) cm^{-1} were assigned to $^6A_1g \rightarrow {}^4T_1g$, $^6A_1g \rightarrow {}^4T_2g$, and $^6A_1g \rightarrow {}^4A_1g + {}^4Eg$ transition, the magnetic moment value was 5.72 BM suggesting an octahedral geometry.

Co (II)-PAAG complex, the greenish blue Co-complex, showed three bands in the visible region with an average of 17391cm^{-1}. This value was assigned to transition $^4A_2 \rightarrow {}^4T_{1\,(P)}$ [26]. This transition was known to be triplet in the divalent cobalt of the Td system[27, 28] Scheme 3b, while υ_1 $^4A_2 \rightarrow {}^4T_2$ and υ_2 $^4A_2 \rightarrow {}^4T_{2(F)}$ could not be seen in the range of this instrument scale, the second transition υ_2 was calculated and found to be 5160 cm^{-1} from reference to Tanabe-Sugano Diagrams of Td geometry, the magnetic moment was 5.2 BM.

The spectrum of Ni(II) complex yellowish green (NiL) showed three bands at 890, 640, and 407 nm (11236, 15625, and 24570) cm^{-1} was assigned to $^3A_2g \rightarrow {}^3T_2g$, $^3A_2g \rightarrow {}^3T_1g_{(F)}$ and $^3A_2g \rightarrow {}^3T_1g_{(P)}$ transition respectively, the magnetic moment value is 2.3, suggesting an octahedral geometry[29].

The spectrum of Cu (II) complex yellowish green (CuL) showed two bands at 894, 315, and 229 nm (11186, 31746, and 43668) cm^{-1}, was assigned to $^2E\ g \rightarrow {}^2T_2g$ and C.T transition, the magnetic moment value is 1.2 BM suggesting an octahedral geometry Scheme 3a [30,31].

Zn (II) and Cd (II): finally, the magnetic moment value was diamagnetic for both Zn (II) and Cd (II) complexes (ZnL) and (CdL), which was attributed to the metal-to-ligand charge transfer, but the spectra showed no d-d electronic transitions in the visible region. The absorption bands were 350 and 291 nm (28571, 34364) cm^{-1} and 301, 260 nm[32].

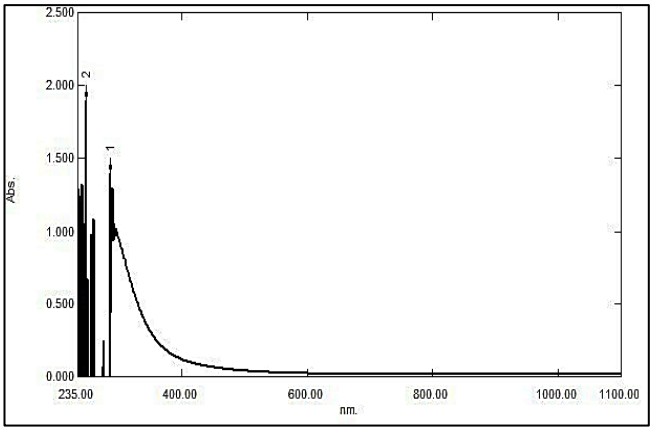

(a)

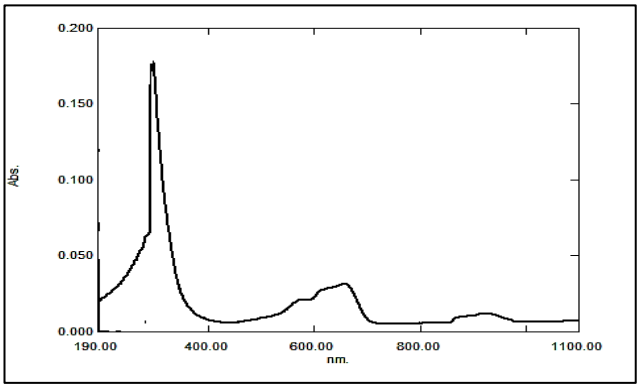

(b)

Figure 2. Electron spectrum of (a) PAAG ligand and (b) CoL complex

2024, 21(9): 2838-2852
https://doi.org/10.21123/bsj.2024.8591
P-ISSN: 2078-8665 - E-ISSN: 2411-7986
Baghdad Science Journal

Table 2. Physical properties of the ligand and its complexes

Comp.	λnm	ύcm⁻	Assignments	Molar cond.	μ*eff* (B.M)	Structure
	286	34965	(n→ π*)			
L	248	40322	π→ π*			
Cr-L	820	12195	$^4A_2g \rightarrow {}^4T_2g$	3.5	3.8	Octahedral
	670	14925	$^4A_2g \rightarrow {}^4T_1g$			
	460	21739	$^4A_2g \rightarrow {}^4T_1g$			
Mn-L	850	11765	$^6A_1g \rightarrow {}^4T_1g(G)$	9.6	5.1	Octahedral
	520	19231	$^6A_1g \rightarrow {}^4T_2g(G)$			
	380	26316	$^6A_1g \rightarrow {}^4A_2g+{}^4Eg(G)$			
Fe-L	701	14265	$^6A_1g \rightarrow {}^4T_1g$	17.4	5.7	Octahedral
	590	16949	$^6A_1g \rightarrow {}^4T_2g$			
	339	29499	$^6A_1g \rightarrow {}^4A_1g+{}^4Eg$			
Co-L		From IR 3438	$^4A_2 \rightarrow {}^4T_2$	3.3	5.2	Tetrahedral
		5160 (cal)	$^4A_2 \rightarrow {}^4T_1(F)$			
	575	17391	$^4A_2 \rightarrow {}^4T_1(P)$			
Ni-L	890	11236	$^3A_2g \rightarrow {}^3T_2g$	9.6	2.3	Octahedral
	640	15625	$^3A_2g \rightarrow {}^3T_1g(F)$			
	407	24570	$^3A_2g \rightarrow {}^3T_1g(p)$			
Cu-L	894	11186	$^2Eg \rightarrow T_2g$	6.5	1.2	Octahedral
	315	31746	C.T			
	229	43668	Intra ligand			
Zn-L	350	28571	C.T	3.1	Diam.	Octahedral
	291	34364	Intra ligand			
Cd-L	301	33223	C.T	5.3	Diam.	Octahedral
	260	37594	Intra ligand			

Table 3. Electronic spectra, spectral parameters, molar conductivity, and μ*eff* of L- metal complexes

Compounds	M p °C (dec) °C	Color
L	260-262	Yellowish brown
CrL	180-182	Olive
MnL	230-232	Pink
FeL	160-162	Brown
CoL	210-212	Blue
NiL	196-198	Yellowish green
CuL	120-122	Yellowish green
ZnL	220-222	Beige
CdL	250-252	Off-white

HNMR spectrum

Nuclear magnetic resonance spectroscopy (^{1}H NMR) [33] is essential for studying substances and their structures. The ^{1}H-NMR technique was used to characterize the synthetic polymer. Fig. 3 and Table. 4 showed that the methylene protons in the PAAG structure corresponded to a signal at 1.16–1.8 ppm and 2.0–2.5 ppm proton of –CH group st 3.31-3.8 ppm [34]. For describing the influence of the solvent on the N-H hydrogen NMR chemical shifts, amide-containing compounds were among the best examples[35]. The spectrum of the copper-ligand complex revealed this change to be true, namely at the amide group. In addition, the azomethine proton (CH=N) was moved up field in the Cu-PAAG complex spectrum, which is indicative of a bond being formed with the Cu center and can be seen as a signal in the region of 7.71 -8.34 ppm in the free Schiff base[36, 37]. The presence of the acrylamide chain, and hence the occurrence of polymerization to generate the desired product, was confirmed by the ^{1}HNMR spectrum.

2024, 21(9): 2838-2852
https://doi.org/10.21123/bsj.2024.8591
P-ISSN: 2078-8665 - E-ISSN: 2411-7986
Baghdad Science Journal

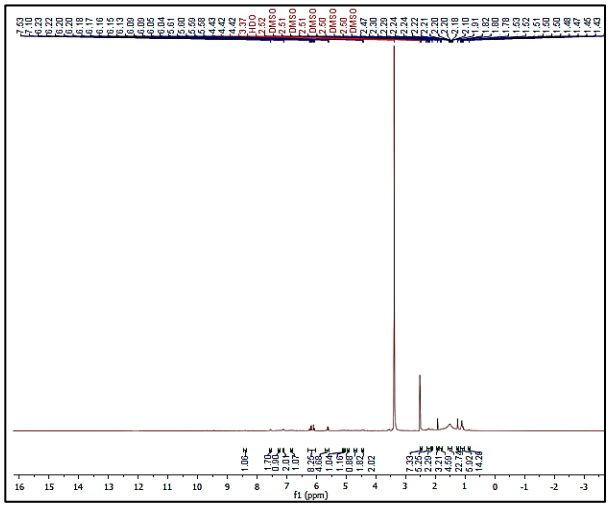

(a)

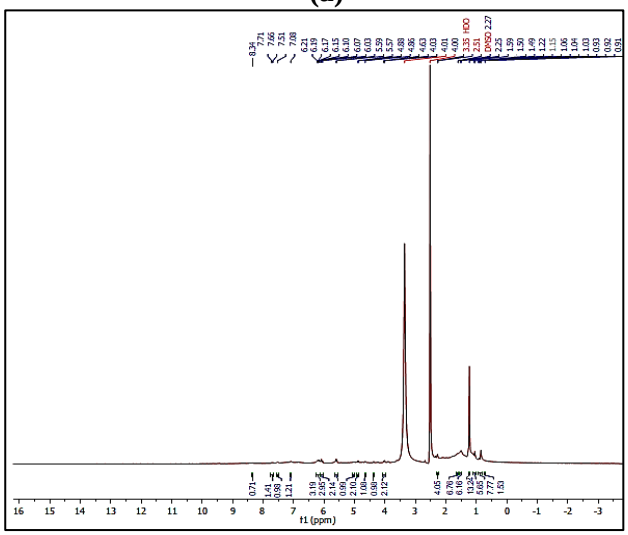

(b)

Figure3. ^{1}HNMR spectrum (300 MHz, DMSO-d$_6$) of (a) L (PAAG) and (b) CuL

Table 4. ^{1}H NMR spectral data of L-PAAG AND CuL complex

Chemical shifts (ppm) for ligand	Chemical shifts (ppm) for CuL complex	Assignments in DMSO
1.16 - 1.8 ppm and 2.0 - 2.5 ppm	1.03 - 1.59 ppm and 2.12 - 2.5 ppm	(-CH_2)methylene protons
3.8 - 3.31ppm	4.0 – 4.8ppm	-CH proton
7.14 -8.25 ppm	7.08 -8.34 ppm	Izomethine proton (CH=N)

Thermal Gravimetric Analysis (TGA)

Thermogravimetric analysis (TGA) is frequently used to understand the effects of temperature and time on the weight of polymeric materials. Polymeric materials can undergo weight changes due to decomposition, oxidation reactions, and physical processes, including sublimation, evaporation, and desorption[38]. TGA-curve of two PAAG-complexes as illustrated in Fig. 4. and Table 5 Results of CuL's TGA presented a progression through three weight-reduction stages. At 110 °C, a weight reduction was 10% in the first stage. This portion of the mass loss was thought to be attributable to water loss through evaporation. This could result from moisture removal or the loss of bound water[39].

Ammonia was released upon heating the PAAM to 244.37 °C, corresponding to the thermal degradation of the organic matter, where the second stage was noticed at 112-400°C with a weight loss of 39%, which may be attributed to the thermal decomposition of the amide and carboxylate side groups of the polyacrylamide[40]. In the third phase, polymer breakdown caused a loss of 46% at 400-900 °C [41]. TGA results for FeL demonstrated weight loss occurring in three distinct phases; the first stage, at 110°C, was associated with a weight reduction of 11%. The water loss at this point was thought to be due to evaporation. The second stage was at 200-400°C with a weight-percent-loss 23 %. In this phase of the weight loss process, the imide group and the M-Cl link were broken down, resulting in the emission of both Co and Cl [42]. Weight loss equaling 46% of the initial total occurred in the third stage, which began at ~400 °C due to the disintegration of Imide groups and the degradation of the polymer main chains[43]. At temperatures above 450°C, the copolymers completely broke down; however, at 900°C, 20% of PAM's mass remained, a result of the decomposition of the Schiff base bond accompanied by a loss of mass that pointed to the ongoing degradation of the polymer into its component monomers, acrylamide and glutaraldehyde [44,45].

Table 5. Thermal analyses data for CuL and FeL

Comp.	Dissociation stages	Temp range in °C	Weight loss Found (Cal)%
CuL	StageI	20-112	10
	StageII	112-400	39
	StageIII	400-900	46
FeL	StageI	20-110	11
	StageII	110-400	23
	StageIII	400-900	46

2024, 21(9): 2838-2852
https://doi.org/10.21123/bsj.2024.8591
P-ISSN: 2078-8665 - E-ISSN: 2411-7986
Baghdad Science Journal

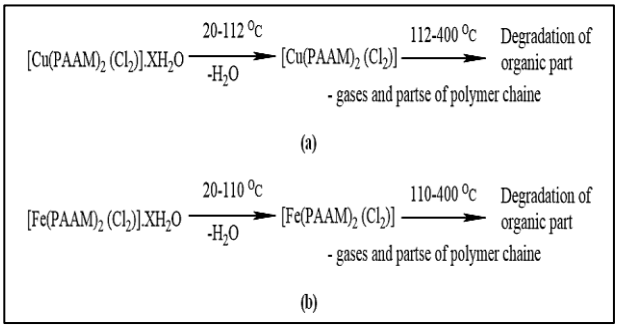

Scheme 2. Thermal behavior of a. CuL b. FeL complexes

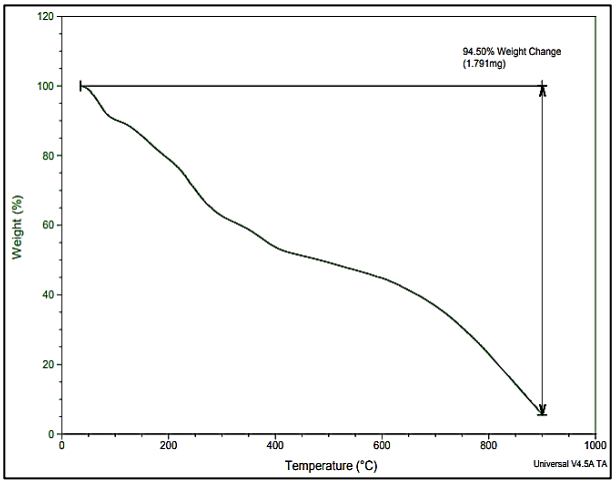

(a)

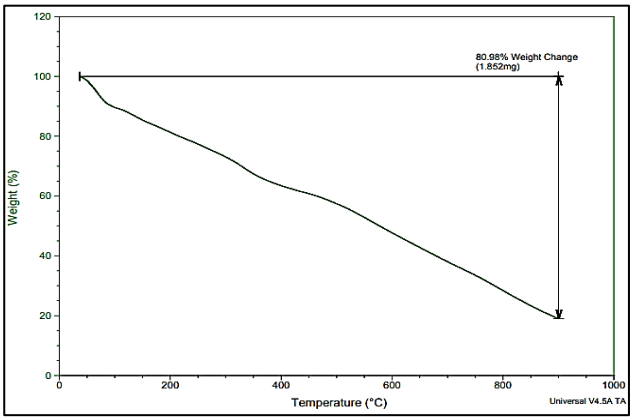

(b)

Figure 4. TGA analysis for (a) CuL and (b) FeL

X-Ray Diffraction analysis

X-ray diffraction helps investigate nanoparticles[46]. X-ray diffraction studies were performed on a category of Schiff's base ligands. The Nanoscale feature of Cd(II), Cr(II), and Ni(II) complexes was demonstrated by the sharp peaks they showed. Comparatively distinct peaks at 2Θ (16, 18.5, 21, 25, 30.5, 32, 34, 35.5, and 37.5) were observed for the NiL Nano complex, but for the CdL and CrL Nano complexes, the spectra were entangled, and the unique peaks had vanished. Probably, X-ray spectroscopy cannot solve it because of the shielding effect of the represented polymer (ligand) molecules [47] Fig. 5.

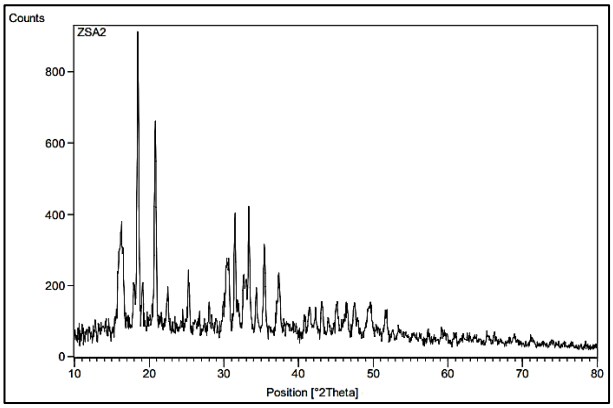

Figure 5. XRD patterns of Nano NiL complex.

Atomic Force Microscopy (AFM)

This method measures the forces exerted by a sharp cantilever tip on a surface at a very close distance, yielding two- and three-dimensional pictures of the surface at the Nanoscale[46]. 3D and two-dimensional pictures of Nano (CrL, NiL, and Cd) complexes were taken using SEM Fig. 6. For these complexes, the granularity accumulation distribution charts were displayed and shown in Fig. 7. The diameter dispersion of NiL with a mean diameter is ranging from 2.25-3.25 nm and an average diameter of 70 nm. The diameters of the particles making up the CrL Nano complex range between 60-100 nm, with an average diameter of 102 nm, and CdL Nano complex particles have a mean diameter ranging from 8-12 nm and an average diameter of 69.59 nm. as shown in table 6.

Table 6. Summary of the AFM information for CrL, FeL, and CdL nano complexes

Sample	Roughness Average (nm)	Root Mean Square (nm)	Average Hight (nm)	Average Diameter (nm)
CrL	5.7	7.7	38.55	102
NiL	1.11	1.57	9.1	70
CdL	1.32	2.05	11.58	60.59

2024, 21(9): 2838-2852
https://doi.org/10.21123/bsj.2024.8591
P-ISSN: 2078-8665 - E-ISSN: 2411-7986
Baghdad Science Journal

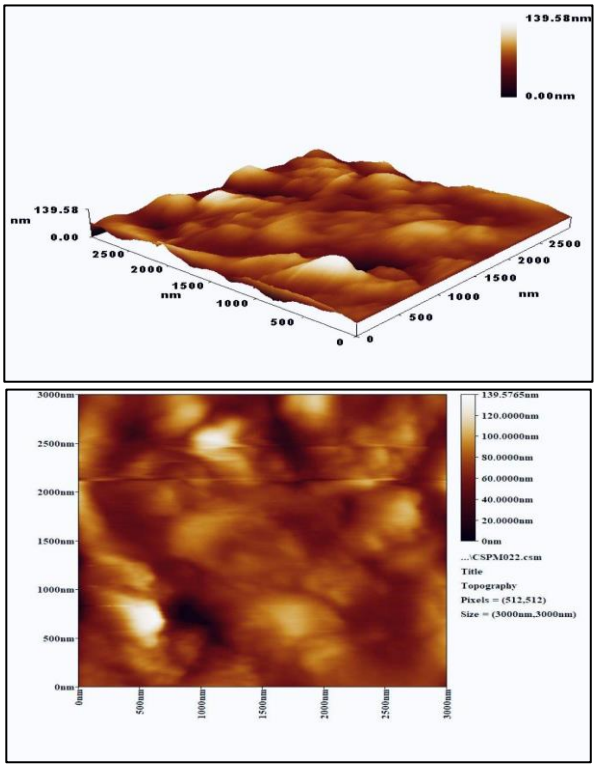

(a)

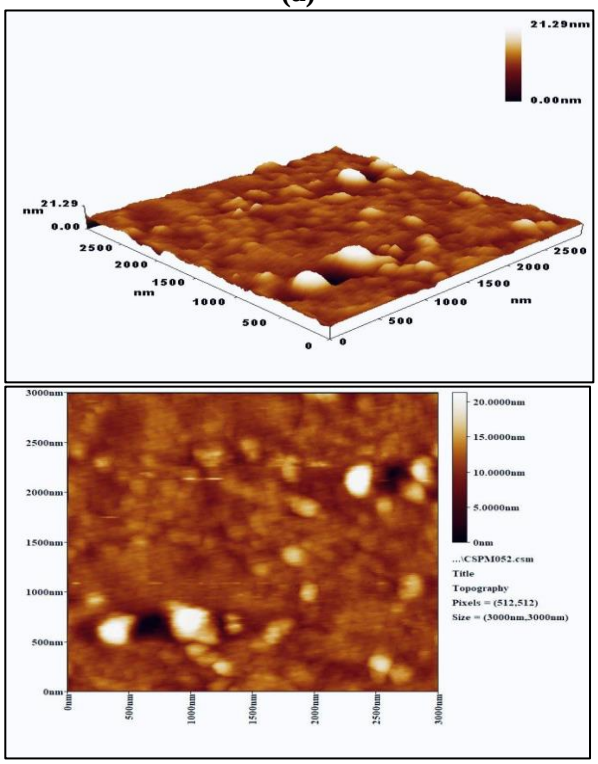

(b)

Figure 6. AFM three-dimensional and tow dimensional image for (a) CrL (b) CdL nanoparticles complexes.

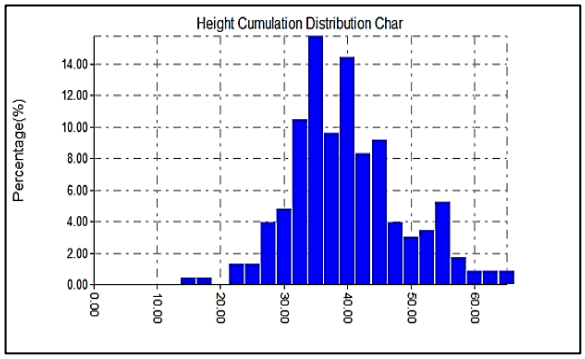

(a)

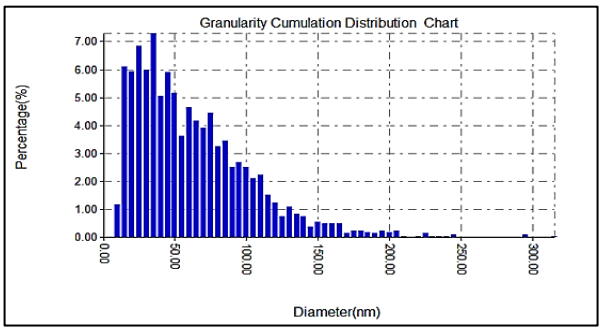

(b)

Figure 7. Granularity accumulation distribution of (a) CrL (b) CdL nanoparticles complexes

Scanning Electron Microscopy (SEM) and Energy Distributed X-Ray Spectrometry (EDS)

Pictures of the NiL nano complex were taken using a scanning electron microscope (SEM), revealing particles with sizes ranging from around 15-51 nm Fig. 8. Similar results were seen for the CdL and CrL nano complexes. In addition, scanning electron microscopy (SEM) pictures of the CrL Nano complex were displayed, revealing particle sizes of around 35-46 nm. Moreover, scanning electron micrographs of the CdL Nano complex revealed around 20-147 nm particle sizes Fig. 9.

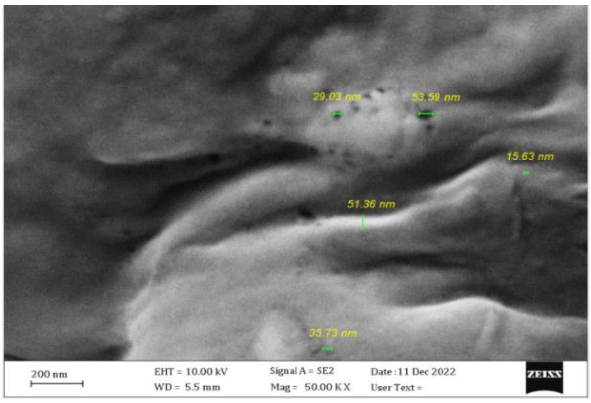

(a)

2024, 21(9): 2838-2852
https://doi.org/10.21123/bsj.2024.8591
P-ISSN: 2078-8665 - E-ISSN: 2411-7986
Baghdad Science Journal

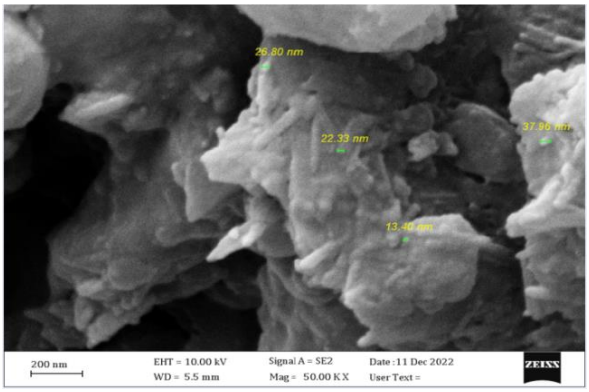

(b)

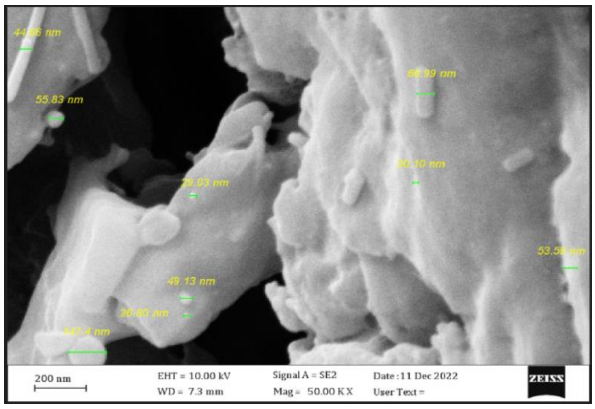

(c)

Figure 8. SEM of (a) NiL (b) CrL (c) CdL nanoparticles complexes.

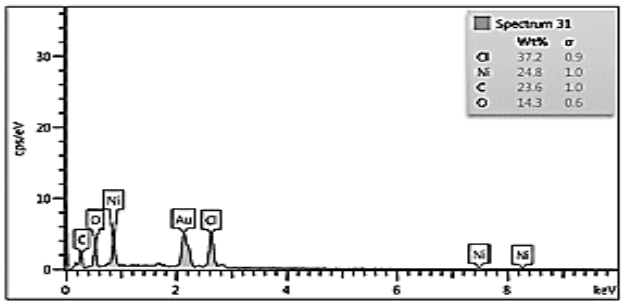

(a)

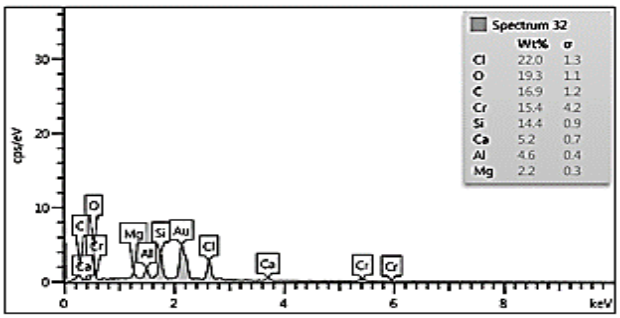

(b)

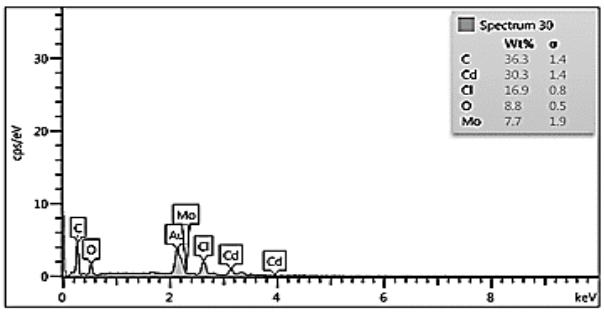

(c)

Figure 9. EDS of (a) NiL (b) CrL (c) CdL nanoparticles complexes.

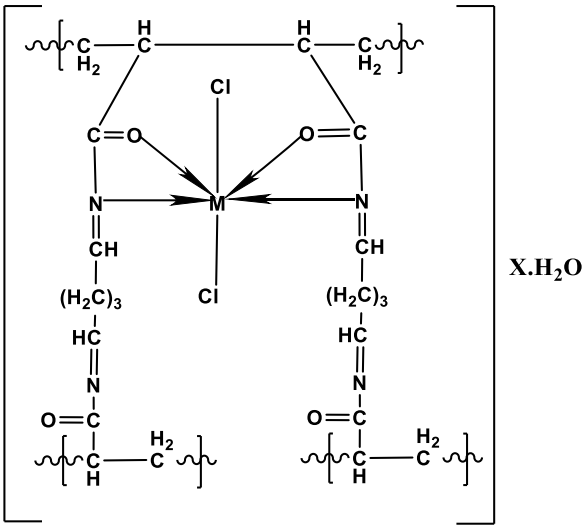

(a) M= Cr, Mn, Fe, Ni, Cu, Zn, Cd

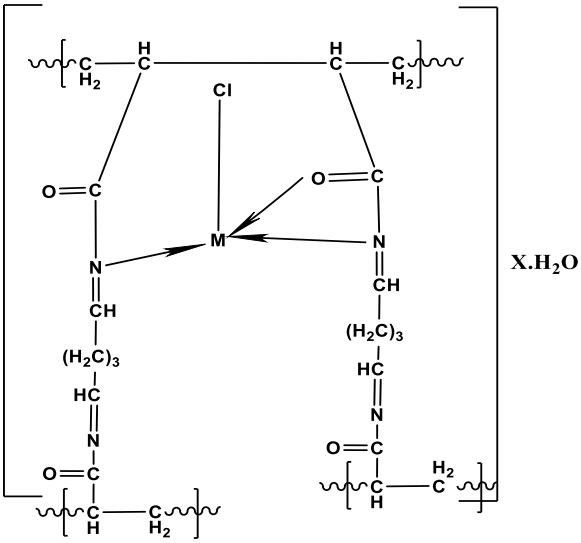

(b) M= Co

Scheme 3. The geometrical structure of a. Octahedral [ML_2 (Cl_2)].XH_2O b. Tetrahedral [ML_2Cl].XH_2O

Application of PAAG to remove elements from contaminated water

Various traditional and membrane approaches are available for removing heavy metal pollutants from wastewater. Contaminated Heavy metal must be removed to stop further contamination and gain economic benefit [48]. An internal standard method (In) and a multi-standard calibration method were used to analyze metals in water samples [49- 51] precisely.

PAAG was applied to remove some of the polluting elements of the water left over from the power stations, where very trace concentrations of the elements that had previously been detected in the samples taken from the liquid waste left over from two power stations were prepared, which were 20, 40, and 60 ppm using the atomic absorption technique to determine its percentage after the removal process, which conducted through the preparation of a polymeric composite of each prepared PAAG and zeolite; the results obtained were listed in Table 7.

Table 7. The experimental result of removal metals (Mn (II), Fe (III), Ni (II), and Cu (II)) by designed PAAG- composite.

Metal	Initial concentration ppm.	Final concentration (after applying PAAG) ppm.	Final concentration(after applying PAAG with composite at 40 ppm from each metal)	Concentration ppm. (in the wastewater from Al Doraa power station after application of PAAG with composite)	Concentration ppm. (in the wastewater from South of Baghdad power station after application PAAG with composite)
Mn(II)	20	5.75			
	40	10	13	ND	ND
	60	15.25			
Fe(III)	20	4.43			
	40	9.4	0.23	ND	ND
	60	16.5			
Ni(II)	20	7			
	40	14	16	0.045	0.066
	60	18.5			
Cu(II)	20	6			
	40	11.8	0.06	0.038	0.043
	60	20			

Conclusion

The results presented above indicated the possibility of synthesizing Nanocomposites from complexation between polymeric-based ligand [(2S, 2'S) – N, N' -(pentane-1, 5-diylidene) bis (2- methyl butan amide)] with heavy metals, which were partially soluble in solvents including water, ethanol, and DMSO, and the ability of the PAAG-ligand to complex rapidly with metals, which allowed its application in a general way. It was successful in removing polluting elements from wastewater by two methods of complexation and adsorption; the first method was the direct interaction between the ligand and the metals in the water environment, while the adsorption method zeolite used with the PAAG-ligand to form composite materials. The results of the water examination before and after using the prepared compounds showed that the composite materials removal was many times better, as the concentration recorded was very low. In contrast, the concentrations of some metals completely disappeared from polluted water.

Acknowledgment

The cooperation of the Central Environmental laboratory staff in the Ministry of Environment.

Authors' Declaration

- Conflicts of Interest: None.
- We hereby confirm that all the Figures and Tables in the manuscript are mine. Besides, the Figures and images, which are not mine, have been permitted re-publication and attached to the manuscript.
- Authors sign on ethical consideration s approval.
- Ethical Clearance: The project was approved by the local ethical committee at University of Baghdad.

Authors' Contribution Statement

This work has been done by collaboration between all authors. The above part was completed, the vehicles were prepared, the necessary tests were conducted to estimate them, samples were collected, and practical applications were carried out, in addition to writing the work by Z. S. A, while the work was reviewed and the results checked by S. S.H and S. H.A.

References

1. Sourbh T b, Bhawna S, Ankit V, Jyoti C, Sigitas T, Vijay K T. Recent progress in sodium alginate based sustainable hydrogels for environmental applications. J Clean Prod. 2018; 198: 143-159. https://doi.org/10.1016/j.jclepro.2018.06.259
2. Ashvinder K R, Vijai K G, Adesh KS, Stefan I V, Magda H A, Vijay K T. Water desalination using nanocelluloses/cellulose derivatives based membranes for sustainable future. Desalination. 2021; 520, 115359. https://doi.org/10.1016/j.desal.2021.115359.
3. Mohamed E M, Ebtissam A S, Mohamed A S, Mohamed S A. Removal of radioactive cobalt/zinc and some heavy metals from water using diethylenetriamine/2-pyridinecarboxaldehyde supported on NZVI. Microchem J. 2019; 145: 1102-1111. https://doi.org/10.1016/J.microc.2018.12.032.
4. Isiuku B O, Enyoh C E. Water pollution by heavy metal and Organic pollutants: Brief review of sources, effects and progress on remediation with aquatic plants. Anal Methods Environ Chem J. 2019; 2(3): 5-38. https://doi.org/10.24200/amecj.v2.i03.66.
5. Semla Z, Goc M. Acrylamide: a Common Food Toxin Related to Physiological Functions and Health. Physiol. Res. 2017; 66: 205-217. https://doi.org/10.33549/physiolres.933381
6. Teresa R, Pierpaolo F, Rosa G, Filomena S. Sustainable Removal of Contaminants by Biopolymers: A Novel Approach for Wastewater Treatment. Current State and Future Perspectives. Processes. 2021; 9: 719. https://doi.org/10.3390/pr9040719.
7. David E, Hansjoerg W, Ema Ž, David P, Christian S. Melt Polymerization of Acrylamide Initiated by Nucleophiles: A Route toward Highly Branched and Amorphous Polyamide. Appl poly Mater. 2021; 3: 2010-2026. https://doi.org/10.1021/acsapm.1c00084?ref=pdf.
8. Hai P Z, Jing J C, Wen B J, Yu Q Y, Bo Y Z, Xiao Y L, et al . Synthesis and Mechanical Properties of Polyacrylamide Gel Doped with Graphene Oxide. Energies. 2022; 15: 5714. https://doi.org/10.3390/en15155714.
9. Olivier B, Clément C, Johann K, Frédéric B, Cédrick F, Céline B. Spotlight on the Life Cycle of Acrylamide-Based Polymers Supporting Reductions in Environmental Footprint: Review and Recent Advances. Molecules. 2022; 27: 42. https://doi.org/10.3390/molecules 27010042.
10. Glen R J, Zaidong L, Athina A, Danielle J L, Paul W, Qiang Z, et al. . Rapid Synthesis of Well-Defined Polyacrylamide by Aqueous Cu (0) - Mediated Reversible-Deactivation Radical Polymerization, Macromolecules. 2016; 49: 483−489. https://doi.org/10.1021/acs.macromol.5b01994.
11. Erzhan I K, Yelzhan S O, Zulkhair A M, Ruslan E N, Zhanar O Z, Aktota A M. Applicability of Zeolite from the Daubabinsk and Chankanai Deposits as a Sorbent for Natural Waters. Water. 2023; 15: 2231. https://doi.org/10.3390/w15122231.
12. Veena S, Syed S, Rama G, Irfan A, Rajib B, Nanthini S. Comprehensive Review on Zeolite-Based Nanocomposites for Treatment of Effluents from Wastewater. Nanomaterials. 2022; 12: 3199. https://doi.org/10.3390/nano12183199.

13. Luciano F, Gilberto R, Antônio E. Zeolite Application in Wastewater Treatment. Adsorp Sci Technol. 2022: 1-26. https://doi.org/10.1155/2022/4544104.
14. Begam T, Tomar R S, Nagpa A K, Singhal R. Synthesis of Poly(acrylamide-co-methyl methacrylate-covinyl amine-co-acrylic acid) Hydrogels by Hoffman Degradation and Their Interactions with Acetaminophen. J. App. Polym. Sci. 2004; 94: 40 –52. https://doi.org/10.1002/app.20706.
15. Ahmed G I, Ahmed Z S, Hamada A E, Mahmoud M S. Synthesis of Poly(Acrylamide-Graft-Chitosan) Hydrogel: Optimization of The Grafting Parameters and Swelling Studies. Am J Polym Sci. 2019; 5(2): 55-62. https://doi.org/10.11648/j.ajpst.
16. Nurşen S, Serkan Ö. Synthesis, Characterization and selectivity studies of poly(Acrylamide) incorporating Schiff Bases. Chinese J Polym Sci. 2009; 27(5): 675−683. https://doi.org/10.1142/S0256767909004370.
17. Anacona J R, Juan L R, Juan C. Synthesis, characterization and antibacterial activity of a Schiff base derived from cephalexin and sulphathiazole and its transition metal complexes. Spectrochim. Acta A: Mol Biomol Spectrosc. 2014; 129: 96-102. https://doi.org/10.1016/j.saa.2014.03.019.
18. Acemi A. Polymerization degree of chitosan affects structural and compositional changes in the cell walls, membrane lipids, and proteins in the leaves of Ipomoea purpurea: An FTIR spectroscopy study. Int J Biol Macromol. 2020; 16: 715-722. https://doi.org/10.1016/j.ijbiomac.2020.06.171.
19. Güzin P, Seda H, Mustafa E P. Molecular Structure, Vibrational, Spectral Investigation and Quantum Chemical DFT Calculations of Poly (N-isopropyl acrylamide-co-nbutyl methacrylate). Polym Korea. 2022; 46: 559-565. https://doi.org/10.7317/pk.2022.46.5.559
20. Nurhan G, Bahar B. Synthesis of New Ligands Containing Azomethine Group and Investigation of Antioxidant, Antiurease Activities. J Sci. 2020; 33(3): 662-671. https://doi.org/10.35378/gujs.615818
21. Bouchra E, El Mehdi H, Asmae N, Mohamed B, Linda B, Sava K, et al. New Bi-Nuclear Nickel (II) Complex-Based Salen Schiff Base: Synthesis, Crystal Structure, Spectroscopic, Thermal, and Electrical Investigations. Chemistry. 2022; 4: 1193–1207.http://dx.doi.org/10.3390/chemistry4040080
22. Maged S A, Maha A A, Jawza S A. Physico-Chemical Study of Mn(II), Co(II), Cu(II), Cr(III), and Pd(II) Complexes with Schiff-Base and Aminopyrimidyl Derivatives and Anti-Cancer, Antioxidant, Antimicrobial Applications. Molecules. 2023; 28: 2555. https://doi.org/10.3390/molecules28062555
23. Sanaa A A, Sana H A. Synthesis, Characterization of Chitosan para- hydroxyl Benzaldehyde Schiff Base Linked Maleic Anhydride and the Evaluation of Its Antimicrobial Activities. Baghdad Sci. J. 2022; 19(6): 1265-1275. https://dx.doi.org/10.21123/bsj.2022.5655
24. Mathur N, Jain N, Sharma A K. Synthesis, characterization and biological analysis of some novel complexes of phenyl thiourea derivatives with copper. Open Chem J. 2018; 5(1). http://dx.doi.org/10.2174/1874842201805010182
25. Ali M H, Ahmed O S, Bassem H H, Ahmed Y, Wael M A, Mohamed F M. Green Synthesis, Characterization, Antimicrobial and Anticancer Screening of New Metal Complexes Incorporating Schiff Base. ACS Omega. 2022; 7: 32418−32431. https://doi.org/10.1021/acsomega.2c03911.
26. Figgis B, Hitchman M. Ligand Filed Theory and its Application. J Chem Educ. 2002; 79(9): 1072. https://doi.org/10.5860/choice.38-3916
27. Nuha A A, Naser D S. Synthesis, Characterization, and Biological Activity of New Metal Ion Complexes with Schiff Base (Z)-3((E)-2-Hydroxybenzylidene) hydrazineylidene) indolin-2-one. J Med Chem Sci. 2023; 6(7): 1660-1674. https://doi.org/10.21608/EJCHEM.2022.124768.5552
28. Haneen R A, Sahar S H. Preparation and study of the physical properties of some complexes with Schiff base ligand for cefdinir derivative. Iraqi J Mark Res Consum Prot. 2022; 14(2): 110-120. http://dx.doi.org/10.28936/jmracpc14.2.2022.(13).
29. Shen X, Yang X, Su C, Yang J, Zhang L, Liu B, et al. Thermo-responsive photoluminescent silver clusters/hydrogel nanocomposites for highly sensitive and selective detection of Cr (VI). J Mater Chem. 2018; 6(8): 2088–2094. https://doi.org/10.1039/C7TC04495J
30. Sahar S H, Nafeesa J K, Zahraa A J. Synthesis Theoretical Study, and Biological Evaluation of Some Metal Ions with Ligand "Methyl -6-[2-(4-Hydroxyphenyl) -2-((1-Phenylethylidene) Amino) Acetamido] -2,2-Dimethyl-5—Oxo-1-Thia- 4 -Azabicyclo [3.2.0] Heptane-3- Carboxylate. Baghdad Sci. J. 2022; 20(1): 2078-8665. https://dx.doi.org/10.21123/bsj.2022.6359
31. Al Zoubi W, VianY J, Veyan T S, Al-Hamdani A A S, Suzan D A,Yang Gon Kim et.al. Synthesis and bioactivity studies of novel Schiff bases and their complexes. J phys org chem. 2019; 4004: 1-7. https://doi.org/10.21123/bsj.2022.7289
32. Bayyappagari B, Shaik K P. Ferro and antiferromagnetic properties of MnO 2 and Ce 1− x Mn x O 2 nanoparticles. Appl Phys A. 2018; 124(1): 1–6. https://doi.org/10.1007/s00339-017-1395-2
33. Yan J, Nie W, Zhang H, Xiu Z, Bao Q, Wang H, et al. Synthesis and Performance Measurement of a Modified Polymer Dust Suppressant. Adv Powder Technol. 2020; 31: 792-803. https://doi.org/10.1016/j.apt.2019.11.033.
34. Acikses A, Hekim S, Oksuz F. Spectroscopic and Electronic Properties of a Copolymer and Its Metal Complexes: A Theoretical and Experimental Study. Chem. Phys. 2019; 527: 110469. https://dx.doi.org/10.1016/j.chemphys.2019.110469.

35. Da S, De A. Theoretical Calculations of 1H NMR Chemical Shifts for Nitrogenated Compounds in Chloroform Solution. Chem Phys. 2020; 528: 110479. http://dx.doi.org/10.1016/j.chemphys.2019.110479.
36. Ababneh T S, El-khateeb M, Tanash A K, AL-Shboul T M, Shammout M J, Jazzazi T M, et al. Synthesis, computational, anticancerous and antiproliferative effects of some copper, manganese and zinc complexes with ligands derived from symmetrical 2,2'- diamino -4,4'-dimethyl-1,1'-biphenyl-salicylaldehyde. Pol J Chem Technol. 2021; 23: 7–15. https://doi.org/10.2478/pjct-2021-0002
37. Jazzazi T M A, Ababneh T S, Abboushi E K. Zinc(II) complexes of symmetrical tetradentate Schiff base ligands derived from 2,2'- diamino - 6,6'-dibromo - 4,4' -dimethyl- 1,1' -biphenyl- salicylaldehyde: Synthesis, characterization and computational study. Jordan J Chem. 2019; 14: 81–87.
38. Dilkes H L, Lant P A, Laycock B, Pratt S. The rate of biodegradation of PHA bioplastics in the marine environment: A meta-study. Mar Pollut Bull. 2019; 142: 15–24. http://dx.doi.org/10.1016/j.marpolbul.2019.03.020.
39. Abd El-Salam H M, Mahmoud E S, Ali M E. Novel grafted hydrogel for Iron and ammonia removal from ground water, synthesis and computational chemistry study. Res Sq. 2022; 1: 1-32. https://doi.org/10.21203/rs.3.rs-2042510/v1.
40. Puspitasari T, Darwis D, Pangerteni D S, Oktaviani1 O, Sari M P. Synthesis and characterization of zeolite-g-polyacrylamide (Zeolite-g-PAAM) by using simultaneous irradiation techniqu. J Phys Conf Ser. 2020; 1436: 012069. https://doi.org/10.1088/1742-6596/1436/1/012069
41. Nabila Y, Jakub K, Pawel B, Wlodzimierz K, Piyush S. Electrochemically Initiated Synthesis of Polyacrylamide Microgels and Core-shell Particles. Polym Mater. 2022; 4: 452−462. https://doi.org/10.1021/acsapm.1c01359.
42. Agnieszka G, Tomasz K, Igor M, Witold M. Synthesis, Thermogravimetric Analysis, and Kinetic Study of Poly-N-Isopropylacrylamide with Varied Initiator Content. Polymers. 2023; 15: 2427. https://doi.org/10.3390/polym15112427
43. Abdelaziz E H, Saad D, Ahmed A, Mohammed E, Mohammed B, Sawsan M. Synthesis and Characterization of Polyacrylamide Crosslinked Copolymer for Enhanced Oil Recovery and Rock Wettability Alteration. Int J Oil Gas Coal Eng. 2015; 3(4): 47-59. https://doi.org/10.11648/J.OGCE.20150304.11
44. Hossein S A, Sheida K K, Javad S G, Maryam T. Crosslinked sulfonated polyacrylamide (Cross-PAA-SO3H) tethered to nano-Fe3O4 as a superior catalyst for the synthesis of 1,3-thiazoles. BMC Chem. 2019; 13: 120. https://doi.org/10.1186/s13065-019-0637-0.
45. Peighambardoust S J, Aghamohammadi B O, Foroutan R, Arsalani N. Removal of malachite green using carboxymethyl cellulose-gpolyacrylamide /montmorillonite nanocomposite hydrogel. Int J Biol Macromol. 2020; 159: 1122–1131. https://doi.org/10.1016/j.ijbiomac.2020.05.093.
46. Siva S, Sana S, Kumar A, Venkataramana B, Vijaya K N. Development of poly (acrylamide-co- diallyl dimethyl ammonium chloride) nanogels and study of their ability as drug delivery devices. SN Appl Sci. 2019; 1: 1716. https://doi.org/10.1007/s42452-019-1742-3
47. Alaa A R, Farah M I, Ahmed A, Ekhlas A S, Evon A. Synthesis and photophysical study of divalent complexes of chelating Schiff base. Baghdad J Biochem Appl Bio Sci. 2020; 1: 5-17. https://doi.org/10.47419/bjbabs.v1i01.27
48. Kavitha E, Rajesh M P, Prabhakar S. Removal and recovery of heavy metals from aqueous solution using b-Cyclodextrin polymer and optimization of complexation conditions. Desalin Water Treat. 2018; 12: 219–230. https://dx.doi.org/10.5004/dwt.2018.22783
49. Manuel E, José R, Miquel G, Alberto T, Gretchen T, Keiko S. Removal of Heavy Metal Ions from Wastewater with Poly-ε-Caprolactone-Reinforced Chitosan Composite. Polymers. 2022; 14: 5196. https://doi.org/10.3390/polym14235196.
50. Abolanle S A, John A O O, Oluwaseyi S O, Oladotun W M, Thabo T I N, Bhekie B M. Heavy Metal Speciation, Microbial Study and Physicochemical Properties of Some Groundwaters: A Case Study. Chem Afr. 2020; 3: 211–226. https://doi.org/10.1007/s42250-019-00099-2
51. Saleem E, Sarah A Q, Nadhir A, Salah L Z. Function of Nanomaterials in Removing Heavy Metals for Water and Wastewater Remediation. Envir. 2022; 9: 123. https://doi.org/10.3390/environments9100123

2024, 21(9): 2838-2852
https://doi.org/10.21123/bsj.2024.8591
P-ISSN: 2078-8665 - E-ISSN: 2411-7986
Baghdad Science Journal

إزالة بعض المعادن الثقيلة من المياه الملوثة باستخدام قاعدة شيف جديدة للبولي أكريلاميد مع مركبات النانو زيولايت

زينب صبير عبد السادة[1] ، سحر صبيح حسن[2] ، سناء هتور عواد[2]

[1] وزارة البيئة ، بغداد ، العراق
[2] قسم الكيمياء، كلية العلوم للبنات، جامعة بغداد، بغداد، العراق.

الخلاصة

تضمن هذا العمل تحضير ليكند قاعدة شيف جديدة مشتقة من مادة البولي أكريلاميد والكلوترالديهايد-[(2S, 2'S) – N, N' - (pentane 1, 5-diylidene) bis (2- methylbutan amide)] مع بعض المعادن الثقيلة (Cr^{+3} , Mn^{+3} , Fe^{+3}, Co^{+2}, Cu, Ni^{+2}, Zn^{+2}, Cd^{+2}) لتنتج المعقدات المقابلة. تم تشخيص قواعد شيف ومعقداتها المعدنية بأستخدام طيف الأشعة تحت الحمراء والأشعة المرئية وفوق البنفسجية، والتوصيلية ,وقيم المغناطيسية والتحليل الحراري الوزني وحيود الأشعة السينية ومجهرالمسح الالكتروني ومجهر القوة الذرية. تم استخدام البوليمرات المحضرة في إزالة عدد من العناصر من المياه الملوثة المسحوبة من المياه الصناعية لمحطتي الطاقة الكهربائية في الدورة وجنوب بغداد وتقدير التراكيز الضئيلة لتلك العناصر قبل وبعد استخدام القاعدة المحضرة بواسطة مطيافية الامتصاص الذري.

الكلمات المفتاحية: اكريلاميد, المواد المتراكبة , مياه ملوثة , قاعدة شيف, زيولايت .